

Lawrence Berkeley National Laboratory

LBL Publications

Title

Environmental influences on autocollimator-based angle and form metrology

Permalink

<https://escholarship.org/uc/item/7qt3d40n>

Journal

Review of Scientific Instruments, 90(2)

ISSN

0034-6748

Authors

Geckeler, Ralf D

Křen, Petr

Just, Andreas

et al.

Publication Date

2019-02-01

DOI




10.1063/1.5057402

Peer reviewed

Environmental influences on autocollimator-based angle and form metrology

Cite as: Rev. Sci. Instrum. **90**, 021705 (2019); <https://doi.org/10.1063/1.5057402>

Submitted: 14 September 2018 . Accepted: 12 November 2018 . Published Online: 14 February 2019

Ralf D. Geckeler , Petr Křeň , Andreas Just, Matthias Schumann , Michael Krause, Ian Lacey , and Valeriy V. Yashchuk



View Online



Export Citation



CrossMark



VACUUM SOLUTIONS FROM A SINGLE SOURCE

Pfeiffer Vacuum stands for innovative and custom vacuum solutions worldwide, technological perfection, competent advice and reliable service.

[Learn more!](#)

Environmental influences on autocollimator-based angle and form metrology

Cite as: Rev. Sci. Instrum. 90, 021705 (2019); doi: 10.1063/1.5057402

Submitted: 14 September 2018 • Accepted: 12 November 2018 •

Published Online: 14 February 2019



View Online



Export Citation



CrossMark

Ralf D. Geckeler,^{1,a)}  Petr Křen,²  Andreas Just,¹ Matthias Schumann,¹  Michael Krause,¹ Ian Lacey,³ 
and Valeriy V. Yashchuk³

AFFILIATIONS

¹Physikalisch-Technische Bundesanstalt, Bundesallee 100, 38116 Braunschweig, Germany

²Czech Metrology Institute, Okružní 31, 63800 Brno, Czech Republic

³Advanced Light Source, Lawrence Berkeley National Laboratory, MS 15-R0317, 1 Cyclotron Road, Berkeley, California 94720, USA

^{a)}Email: Ralf.Geckeler@ptb.de

ABSTRACT

Deflectometric profilometers are indispensable tools for the precision form measurement of beam-shaping optics of synchrotrons and x-ray free electron lasers. They are used in metrology labs for x-ray optics worldwide and are crucial for providing measurement accuracy dictated by the form tolerances for modern state-of-the-art x-ray optics. Deflectometric profilometers use surface slope (angle) to assess form, and they utilize commercial autocollimators for the contactless slope measurement. In this contribution, we discuss the influences of environmental parameters, such as temperature and air pressure, including their gradients, on high-accuracy metrology with autocollimators in profilometers. They can cause substantial systematic errors in form measurement, especially in the case of large and strongly curved optical surfaces of high dynamic range. Relative angle and form measuring errors of the order of 10^{-4} are to be expected. We characterize environmental influences by extended theoretical and experimental investigations and derive strategies for correcting them. We also discuss the possibility to minimize the contributions of some errors by the application of sophisticated experimental arrangements and methods. This work aims at approaching fundamental limits in autocollimator-based slope and form metrology.

Published under license by AIP Publishing. <https://doi.org/10.1063/1.5057402>

I. INTRODUCTION

Deflectometric profilometers are highly versatile instruments for the form measurement of reflecting optics that utilize slope (angle) to assess form. For the contactless slope measurement, commercial autocollimators, precision metrology tools with a wide range of applications in research, engineering, and manufacturing,^{1,2} are frequently used. Deflectometric profilometers can measure optical surfaces which, due to their sizes and/or topography gradients, pose a challenge to interferometry. Furthermore, they rely on the straight propagation of light and, therefore, are independent of material flatness standards. Because of these advantages, deflectometric profilometers turned out to be especially suitable for characterizing beam-shaping optical surfaces for beamlines at synchrotrons and x-ray free electron lasers

(XFEL), as well as flatness standards for interferometer calibration at national metrology institutes (NMIs), e.g., Refs. 3–9. Beamline optics feature a challenging combination of large size (up to 1.5 m length), aspherical and rotationally asymmetric shapes, and stringent demands on their form and slope accuracy [2 nm peak-to-valley (pv) in form, 10 milliarcsec or 50 nrad root-mean-squared in slope].^{10–12}

Deflectometric profilometry poses stringent demands on the quality, alignment, and characterization of the profilometer's optomechanical components, including the autocollimator and the pentaprism.^{13–27} When properly aligned, the beam deflection angle of the pentaprism is highly robust regarding changes in its angular orientation.^{16–19} The reflectivity and curvature of the surface under test (SUT) influence the angle response of the autocollimator.¹³ It is also affected by the autocollimator's beam length, which varies

substantially when the SUT is scanned using a movable pentaprism.²⁰⁻²² The shape, diameter, and position of the aperture stop, which is used to restrict the beam footprint on the SUT, are of importance too.^{23-25,13} Finally, the angle response of the autocollimator is also influenced by the sagittal beam deflection perpendicular to the main scanning direction, as it engages its measuring axes simultaneously and results in crosstalk.^{26,27}

The accurate characterization of the systematic angle measuring errors of an autocollimator is a prerequisite for its application to this demanding metrological task.^{28,13} Such a calibration is transferable only if the measuring conditions during the autocollimator's prior evaluation and during its use in the profilometer are identical. Any deviation between conditions leads to errors in the autocollimator's angle response. This work is essential for approaching fundamental limits in the autocollimator-based slope and form metrology of beam-line optics—at which we have not yet arrived. While some of the measuring conditions can be specified in advance and held constant, others are subject to unavoidable changes. With deflectometric profilometers, which use a movable pentaprism to scan the SUT, this is the case of the length of the autocollimator's measuring beam. Additionally, the reflectivity and curvature of the SUT may vary from specimen to specimen. Interlaboratory and intralaboratory changes in environmental parameters may also be present.

In this contribution, we focus on the influence of environmental parameters on the precision angle and form metrology with autocollimators. In Sec. II, we present a simplified analytical model of an autocollimator and its angle measurement, which is utilized in the following sections. In Sec. III, we discuss the impact of environmental parameters on the air's refractive index and on angle metrology with autocollimators in general. In Sec. IV, we focus on the impact of air pressure. While temperature is stabilized and monitored accurately in lab environments, pressure is usually not controlled. It decreases with increasing elevation above sea level and is subject to substantial variation due to weather changes. Pressure exerts a dominant influence on the air's refractive index.²⁹ Based on extended theoretical and experimental investigations, we characterize its impact on angle metrology with autocollimators and provide strategies for correction. In Sec. V, we discuss how air pressure changes influence the high-accuracy form measurement of beamline optics by use of deflectometric profilometers. In Sec. VI, we focus on the impact of gradients in the pressure and temperature of air on

angle and form metrology. In Sec. VII, we illustrate the influence of various temperature-induced changes in the autocollimator itself, such as its thermal expansion and changes in the refractive index of the glass of its objective. Finally, in Sec. VIII, we discuss approaches to the suppression of systematic form measuring errors in deflectometric profilometry.

II. ANGLE METROLOGY WITH AUTOCOLLIMATORS

A. Angle measuring principle

The angle measurement of an autocollimator is based on assessing the shift of an image on a detector, using the autocollimator's objective acting as a lever that translates small angular beam deflections into measurable image shifts in proportion to its focal length.

Figure 1 presents a schematic diagram of the geometrical paths of the outgoing and returning autocollimator beams. We consider an outgoing beam (green) on the autocollimator's optical axis. It is intersected by a SUT, located at a distance D from the front of the autocollimator's objective. The SUT tilt angle, α , results in twice the angle, 2α , of the reflected beam (red), which intersects the objective at a distance $s = D \cdot \tan(2\alpha)$ with respect to its optical axis. We assume that the focal length of the objective, f , and the distance of the sensor from it, L , are not necessarily identical.

We use the thin lens approximation.³⁰ The distance y between the optical axis and the point where the returning beam cuts the detector plane is then given by

$$y = \tan(2\alpha) \cdot \left(L - D \cdot \frac{L-f}{f} \right). \quad (1)$$

The angle reading of the autocollimator, $\tilde{\alpha}$, is derived from y by using the equation $y = \tan(2\tilde{\alpha}) \cdot f_c$, with f_c being the focal length of the objective, which has been stored in the autocollimator's electronics and is used for the conversion of the image shift to angle.

If we make use of the approximation $\tan(2\alpha) \approx 2\alpha$ for small α , the relative angle measuring error η of the autocollimator (the difference between the autocollimator's angle readings $\tilde{\alpha}$ and the real tilt angle α of the SUT, divided by α) is then given by

$$\eta = \frac{\tilde{\alpha} - \alpha}{\alpha} \approx \frac{L-f_c}{f_c} - \frac{L-f}{f} \cdot \frac{D}{f_c}. \quad (2)$$

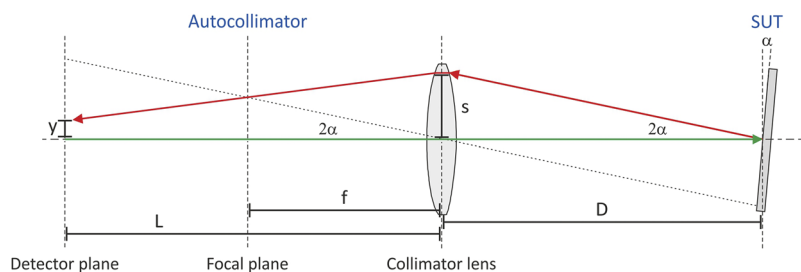


FIG. 1. Schematic diagram of the geometrical paths of the outgoing (green) and returning (red) autocollimator beams. See text for details.

For the investigations presented in this article, we need to distinguish L , f , and f_c . For an ideal autocollimator, however, we may assume that the manufacturer carefully places the detector in the focal plane of the objective during assembly under the given environmental conditions, with $L = f = f_c$. In this case, $\tilde{\alpha} = \alpha$ and $\eta \equiv 0$, i.e., the autocollimator measures tilt angle of the SUT without error.

B. Impact of detector location

If the detector is not located in the focal plane of the autocollimator's objective, then $L \neq f$ and an angle error is introduced, which depends on the distance D between the autocollimator and the SUT, see Eq. (2). Distance-dependent errors are especially relevant to deflectometric profilometers, which use a movable pentaprism to scan the SUT, as the effective distance to the SUT (i.e., the autocollimator beam length) is subject to unavoidable changes.

We assume a constant focal length $f = f_0$ of the autocollimator's objective, which is also used for the conversion of the image shift to angle, so that $f_c = f_0$. We also assume that the detector is initially located in the objective's focal plane, so that $L_0 = f_0$. In this article, we follow the convention that parameters with a subscript refer to specific and constant initial values. When the detector is shifted from L_0 to L , from Eq. (2), we can derive the resulting relative angle measuring error η as

$$\eta = \frac{L - f_0}{f_0} \cdot \left(1 - \frac{D}{f_0}\right). \quad (3)$$

For a detector defocus ($L - f_0 \neq 0$) and a SUT distance $D \neq f_0$, a relative angle measuring error $\eta \neq 0$ is present. Note that, for $D = f_0$, the path of the returning autocollimator beam (red) in Fig. 1 in the autocollimator is parallel to the objective's optical axis. This eliminates the impact of changes in the location of the detector.

If we assume that, in Eq. (3), the term in parentheses is of the order of one and require that the relative error η does not exceed 10 ppm (parts per million), then a detector defocus up to 10 ppm of the autocollimator's focal length f_0 is tolerable. Depending on the focal length, this amounts to a tolerable defocus of a couple of micrometer. Even if the manufacturer has carefully eliminated the detector defocus during the assembly of the autocollimator, it may result from the impact of changing environmental parameters, such as the thermal expansion of the frame on which the objective and the detector are mounted, see Sec. VII B.

C. Impact of the focal length

We now consider changes in the focal length of the autocollimator's objective from an initial value f_0 to f . We assume that the detector is initially located in its focal plane, so that $L_0 = f_0$, and that its distance to the detector is constant, so that $L = L_0$. We also assume that f_0 is used for the conversion of the image shift to angle, so that $f_c = f_0$. When the focal length of the objective changes from f_0 to f , from Eq. (2), we can derive the resulting relative angle measuring error η as

$$\eta = \left(1 - \frac{f_0}{f}\right) \cdot \frac{D}{f_0}. \quad (4)$$

Changes in the objective's focal length are the result of changes in the refractive index of the air (by the temperature, pressure, and humidity of air, see Sec. III) or in the refractive index of the objective's lens glass, see Sec. VII C.

D. Impact of lens aberrations

Despite careful manufacturing, the autocollimator's objective will feature some optical aberrations. An important example of the monochromatic aberrations is the spherical aberration, one of the primary (third-order) Seidel aberrations. It describes the fact that a beam which intersects the lens at a certain distance s with respect to its optical axis is focused at a different focal point when compared to a paraxial beam with $s = 0$. The difference in focal lengths is the longitudinal aberration (LA). Uncorrected positive optical elements, such as a thin, biconvex lens, usually feature an undercorrected spherical aberration, i.e., the focal length for beams passing through the lens at a certain distance to its optical axis is smaller than the paraxial focal length and the LA is negative. For considering the impact of the LA on the relative angle measuring error η of the autocollimator, Eq. (4) can be used. To this purpose, we identify f_0 with the paraxial focal length of the lens and f with the focal length for beams, which intersect the lens at a distance.

The spherical aberration can also be characterized by the transverse aberration (TA). It refers to the lateral displacement of a beam when it intersects the paraxial focal plane and, therefore, is directly proportional to the angle measuring error of the autocollimator. The TA is characterized by $TA \sim s^3$.^{30,31} According to Fig. 1, the returning (red) autocollimator beam passes the lens at a distance $s = D \cdot \tan(2\alpha)$ with respect to its optical axis. For small SUT angles, $TA \sim (D\alpha)^3$. It leads to a third-order angle measuring error of the autocollimator $\tilde{\alpha} - \alpha \sim (D\alpha)^3$.

In our analysis, we are neglecting optical aberrations of the autocollimator's objective. As our focus is on the impact of environmental changes, in this article, the autocollimator's measuring errors are always referenced to the errors before the changes take effect. This procedure eliminates the impact of all error sources, which are not affected by environmental changes, and justifies the use of an idealized autocollimator model.

E. Impact of the beam splitter

In the schematic diagram of the autocollimator, Fig. 1, we have omitted the beam splitter, which allows it to use its objective both for projecting the reticle image into infinity and, after reflection by the SUT, for imaging the reticle onto the detector. We can treat it as a plane parallel plate with a refractive index n_g and thickness d , which is inserted into the path of the returning autocollimator beam (red) after it has passed the objective, see Fig. 1. It displaces the focal plane of the objective along its optical axis by

$$\Delta z \approx d \cdot \frac{n_g - n}{n_g}. \quad (5)$$

Here, n is the refractive index of the air in which the plate is embedded. Equation (5) can be derived from the law of refraction³⁰ by use of $\tan u \approx \sin u \approx u$ for $u \ll 1$. Note that, at least for small SUT angles α , Δz does not depend on α . The plane parallel plate, therefore, displaces the focal plane of the autocollimator's objective. It does not, however, affect the objective's focal length.

We do not need to consider the displacement of the focal plane of the autocollimator's objective as long as we identify the detector defocus $L - f$ on the right-hand side of Eq. (2) as the distance between detector plane and the actual (displaced) focal plane. We will, however, consider the impact of environmental changes on the beam splitter in Sec. VII E.

F. Impact of SUT distance

In Secs. II B and II C, we have derived the relative angle measuring error η of an—initially perfectly adjusted—autocollimator in the case of varying a single parameter, while the other parameters are held constant. Equation (3) describes the impact of displacing the detector with respect to the objective's focal plane. The relative angle measuring error η then shows a dependence on the SUT distance D of the functionality $(1 - D/f_0)$. Equation (4) describes the impact of changing the focal length of the objective. The relative error η then shows a functionality D/f_0 . Furthermore, in Sec. VII E, we consider a temperature-induced effect, which shows no dependence on D at all. In the case of deflectometric profilometers, which use a movable pentaprism to scan the SUT, D is highly variable. In Sec. V, we discuss the implications for the deflectometric form measurement.

Note that when an autocollimator is used at different SUT distances D , optical aberrations of its objective may become a significant error source. As we have pointed out in Sec. II D, the autocollimator's measuring errors are always referenced to the errors before the environmental changes take effect. Errors that are independent of environmental parameters, such as optical aberrations of the autocollimator's objective, are then eliminated.

III. THE REFRACTIVE INDEX OF AIR

A. Dependence on environmental parameters

The Edlén equation^{32,33} describes the refractive index of air $n(t_{90}, p, p_f)$ as a function of the temperature t_{90} [according to the international temperature scale of 1990 (ITS-90) temperature scale], air pressure p , and humidity in terms of the partial pressure p_f of water vapor. Environmental data logged every 5 min in Physikalisch-Technische Bundesanstalt (PTB), Germany clean room center over an entire year (2015) show peak-to-valley variations of 0.06 °K for t_{90} , 69 hPa for p , and 5.7 hPa for p_f . These result in variations of n of 0.06 ppm, 18.52 ppm, and 0.21 ppm, respectively, for the central wavelength of

640 nm of a red light-emitting diode (LED). The partial derivatives of n with respect to t_{90} , p , and p_f are -0.925 ppm/K, 0.268 ppm/hPa, and -0.036 ppm/hPa, respectively.

While temperature is stabilized and monitored accurately in laboratory environments, pressure is usually neither controlled nor recorded. It decreases with increasing elevation above sea level and is subject to substantial variation due to weather changes. Pressure, therefore, exerts a dominant influence on the air's refractive index, as is demonstrated by the numbers cited above. Its impact on the refractive index of air is approximately two orders of magnitude larger than those of temperature and humidity. Note, however, that PTB's clean room center features an exceptional temperature stability. When larger temperature changes are present, temperature also needs to be taken into consideration, see Sec. VII.

In most instances, the influence of humidity can be neglected and we may focus on the impact of pressure and temperature changes. As the deviation of the refractive index of air from one is proportional to the number density of molecules and, therefore, proportional to pressure p and inversely proportional to temperature T , we may then use the approximation

$$\frac{n-1}{n_0-1} \approx \frac{p}{p_0} \cdot \frac{T_0}{T}. \quad (6)$$

Here, we use the notations $n = n(T, p)$ and $n_0 = n(T_0, p_0)$.

B. Impact on angle metrology with autocollimators

The focal length of a lens depends on its geometry and on the ratio of the refractive indices of its bulk material, n_g , and of the air, n , in which it is embedded. For a simpler analytical derivation, we use the thin lens approximation.³⁰ When the refractive index of air changes from n_0 to n , the related change in the focal length of the lens from f_0 to f is given by

$$\frac{f}{f_0} = \frac{n}{n_0} \cdot \frac{n_g - n_0}{n_g - n}. \quad (7)$$

In Sec. II C, we have considered changes in the focal length of the autocollimator's objective under the assumption that, under the given environmental conditions during its assembly (especially p_0 and T_0), the autocollimator is adjusted perfectly. When the refractive index of air changes from n_0 to n , by use of Eqs. (4) and (7), the related change in the relative angle measuring error η of the autocollimator can be derived as

$$\eta = \frac{n - n_0}{n} \cdot \frac{n_g}{n_g - n_0} \cdot \frac{D}{f_0}. \quad (8)$$

From Eqs. (6) and (8), we can derive the relative angle measuring error η as a function of the air's pressure p and temperature T at a constant humidity as

$$\eta \approx (n_0 - 1) \cdot \left(\frac{pT_0}{p_0T} - 1 \right) \cdot \frac{n_g}{n_g - n_0} \cdot \frac{D}{f_0}. \quad (9)$$

To obtain a clearer representation of the equation, we made use of a numerically insignificant approximation based on $(n_0 - 1) \ll 1$.

IV. IMPACT OF AIR PRESSURE ON ANGLE METROLOGY WITH AUTOCOLLIMATORS

A. Theory and experimental validation

In this section, we analyze the impact of air pressure changes on the angle metrology by using autocollimators. We assume a constant temperature $T = T_0$ and humidity of the air. When its pressure changes from p_0 to p , from Eqs. (4) and (6), the resulting relative angle measuring error η follows as

$$\eta = c \cdot \frac{p - p_0}{p_0} \cdot \frac{D}{f_0}, \quad (10)$$

with the sensitivity c given by

$$c = (n_0 - 1) \cdot \frac{n_g}{n_g - n_0}. \quad (11)$$

In Ref. 29, we investigated the sensitivity c of an autocollimator type Elcomat 3000, manufactured by Möller Wedel Optical (MWO),³⁴ which is used in most deflectometric profilometers. We applied ray tracing of the autocollimator based on design data provided by MWO and performed experimental investigations with PTB's novel Spatial Angle Autocollimator Calibrator (SAAC), its primary angle standard WMT 220, and with the Interferometric Small Angle Generator (IGMU) of the Czech Metrology Institute (CMI).

The values for the pressure sensitivity obtained by use of the simple Eq. (11), by ray trace modeling, and by extensive experimental investigations, demonstrated a high degree of consistency. Experimentally, different specimens of the Elcomat 3000 were investigated at different SUT distances. We evaluated a sensitivity of $c = 7.6 \cdot 10^{-4}$ and an associated standard uncertainty³⁵ of $u_c \approx 0.5 \cdot 10^{-4}$. By use of $p_0 = 1013.25$ hPa at sea level, we can evaluate the pressure sensitivity $c/p_0 = 7.5 \cdot 10^{-7}$ per 1 hPa change in air pressure, or 0.75 ppm/hPa (ppm: parts per million), and its associated uncertainty $u_{c/p_0} \approx 0.05$ ppm/hPa. Here, $\partial\eta/\partial p = c/p_0$, multiplied by the distance-dependent term in Eq. (11).

Figures 2 and 3 present experimental data obtained with an Elcomat 3000 autocollimator. The distance between the SUT and the front end of the autocollimator's lens barrel was 1000 mm. Note that, with the Elcomat 3000, the distance between the barrel's front end and the principal plane of the objective facing it is 21.5 mm. This results in a total SUT distance of approximately $D = 1022$ mm, so that $D/f_0 \approx 3.4$.

According to Eqs. (2) and (10), a change in air pressure results in a concomitant angle measuring deviation of the autocollimator (i.e., a difference between the measured and the real SUT angle), which is proportional to the pressure change and to the angle itself. Therefore, when the autocollimator's measuring deviation is plotted as a function of angle, two data sets obtained at different ambient air pressures differ from each other by a linear function, i.e., their slopes are different.

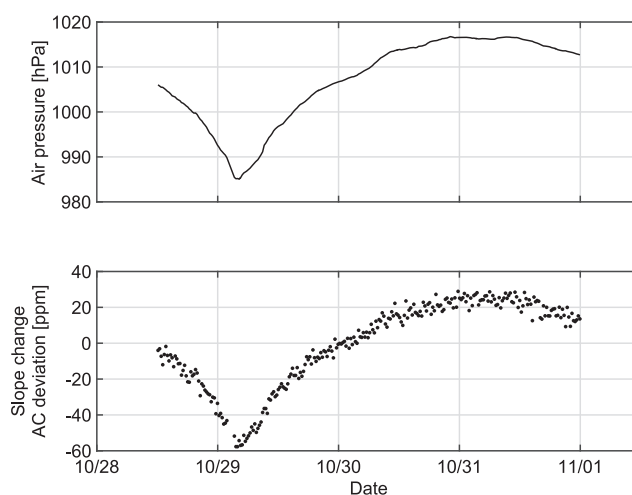


FIG. 2. Concomitant changes in ambient air pressure (upper graph) and the slope of a line fitted to the autocollimator's measuring deviation (lower graph) as a function of time. A SUT distance $D = 1022$ mm was selected, so that $D/f_0 \approx 3.4$.

For the autocollimator type Elcomat 3000, our experimental data confirm the idealized model, which we use in this article for distances D up to 1022 mm over the entire measuring range of ± 1000 arc sec (± 4.85 mrad). Only at a distance $D = 1722$ mm, for angles larger than ± 400 arc sec (± 1.94 mrad), a third-order component in the autocollimator's measuring deviations became noticeable in response to pressure changes. It will be addressed by ray trace modeling in the future. For the derivations in this article, however, the idealized model proves to be adequate. It allows us to derive compact analytical expressions for all effects.

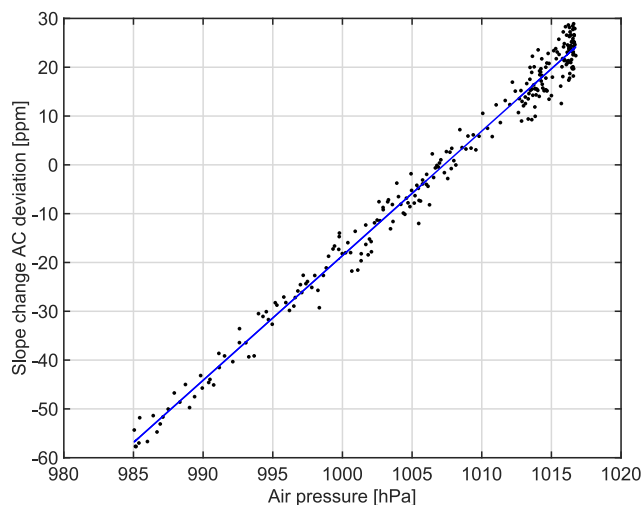


FIG. 3. The slope of the autocollimator's measuring deviation as a function of air pressure, as derived from the data presented in Fig. 2, together with a best-fit line (blue).

B. Pressure changes due to weather

The ambient air pressure changes substantially with weather and depends on the elevation above sea level. We could characterize weather-related pressure changes by use of unique long-term (2006–2016) environmental data recorded at 5 min intervals at the clean room center of PTB (Braunschweig, Germany). From the decade-long data set, a peak-to-valley variation of 84 hPa was observed, with the air pressure obeying a normal distribution with a standard deviation of 9.2 hPa, see Ref. 29 for a detailed analysis.

C. Pressure changes due to elevation

For deriving the pressure of the air as a function of the elevation h in the lower troposphere ($h < 11$ km), we make use of the International Standard Atmosphere (ISA):³⁶

$$p(h) = p_{0,ISA} \cdot \left(1 - \frac{L_b h}{T_{0,ISA}}\right)^{\frac{g_0 M}{R_0 L_b}}, \quad (12)$$

with $p_{0,ISA} = 1013.25$ hPa, $T_{0,ISA} = 288.15$ K, the temperature lapse rate $L_b = 0.0065$ K/m, the gravitational acceleration $g_0 = 9.80665$ m/s², the molar mass of dry air $M = 0.0289644$ kg/mol, and the universal gas constant $R_0 = 8.31447$ J/(mol · K). By use of Eq. (12) or Eq. (28), we can derive a pressure gradient of $\partial p / \partial h = -0.12$ hPa/m.

In the case of our recent key comparison on autocollimator calibration, EURAMET.L-K3.2009, which involved 25 international labs, elevations above sea level ranged from -2 to 712 m.³⁷ According to Eq. (12), these resulted in a pressure difference of 89 hPa. For the standard of the comparison, an autocollimator type Elcomat 3000, this corresponds to an angle measuring error at the margins of its measurement range (± 1000 arc sec or ± 4.85 mrad) of ± 0.07 arc sec ($0.34 \mu\text{rad}$), multiplied by D/f_0 . Pressure variation due to differences in elevation, therefore, represent a substantial error source.

D. Correcting pressure changes

For correcting the autocollimator's angle measurements $\tilde{\alpha}$, obtained at an air pressure p_1 , to a different pressure level p_2 , we use Eqs. (10) and (11) to obtain

$$\tilde{\alpha}(\alpha, p_2) = \tilde{\alpha}(\alpha, p_1) + \tilde{\eta} \cdot \alpha, \quad (13)$$

with

$$\tilde{\eta} = c \cdot \frac{p_2 - p_1}{p_m} \cdot \frac{D}{f_0}. \quad (14)$$

Here, p_m is the pressure at which the detector of the autocollimator is located in the focal plane of the autocollimator, i.e., it is the pressure at the time of the assembly and adjustment of the autocollimator by the manufacturer, see Sec. III B. Note that, in the divisor of Eq. (14), p_m can usually be replaced by either p_1 or p_2 with negligible numerical impact.

V. IMPACT OF AIR PRESSURE ON DEFLECTOMETRIC FORM MEASUREMENT

Figure 4 presents a schematic diagram of the most common type of deflectometric profilometer. A pentaprism directs

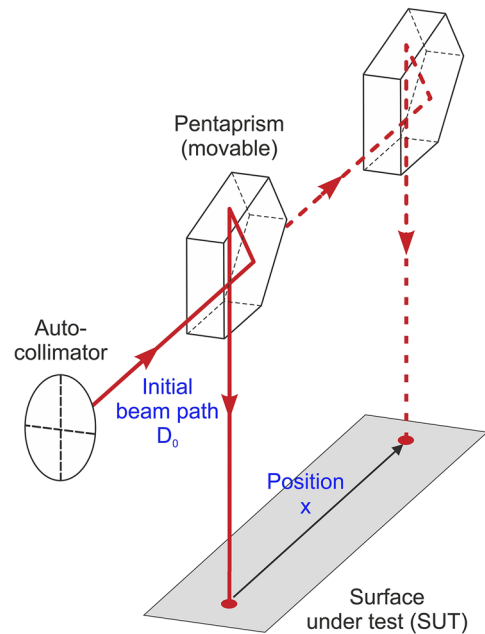


FIG. 4. Schematic diagram of the most common type of deflectometric profilometer. A movable pentaprism deflects the outgoing autocollimator beam onto the SUT at different scanning positions.

the outgoing autocollimator beam by 90° toward the SUT. By moving the prism, the beam footprint on the SUT can be moved to different scanning positions. Usually, to improve lateral resolution, a small (mm-sized) aperture, which comoves with the prism, restricts the beam footprint. The SUT reflects the beam back to the autocollimator, which measures the beam deflection angle at each position. The SUT topography is obtained by integrating the slope (angle).

To investigate the dominant influence of air pressure on the form measurement of an optical surface by a deflectometric profilometer, we assume the measurement of a spherical SUT of radius r with its topography profile $z(x)$ given by

$$z(x) = r - (r^2 - x^2)^{\frac{1}{2}} \quad (15)$$

in Cartesian coordinates x - z . For $(x/r) \ll 1$, by making use of $(1 - u)^{1/2} \approx 1 - u/2$ for $u \ll 1$, the spherical profile can be approximated by a parabolic profile with its topography $z(x)$ defined by

$$z(x) = \frac{x^2}{2r}, \quad (16)$$

with its local surface slope $\alpha(x)$ given by

$$\alpha(x) = \frac{\partial z}{\partial x} = \frac{x}{r}. \quad (17)$$

By use of Eq. (10), the difference between the real topography profile $z(x)$, measured at a ambient air pressure p_0 (at which the autocollimator is assumed to provide an error-free angle measurement), and the profile $\tilde{z}(x)$, measured at a pressure

p , can then be obtained by integration of the slope angles of the SUT,

$$\tilde{z}(x) - z(x) = c\kappa \cdot \int_0^x \frac{x}{r} \cdot \frac{x + D_0}{f_0} dx, \quad (18)$$

with the following notation for the relative pressure difference:

$$\kappa = \frac{p - p_0}{p_0}. \quad (19)$$

D_0 denotes the initial beam path length at the position $x = 0$, which results from various beam paths between the optomechanical components and inside the pentaprism, see Fig. 4. The topography measuring error is then given by

$$\tilde{z}(x) - z(x) = \frac{c\kappa}{f_0 r} \cdot \left(\frac{x^3}{3} + D_0 \frac{x^2}{2} \right). \quad (20)$$

If we assume an ideal case with initial beam path length $D_0 = 0$, by use of Eqs. (20) and (17), the relative slope measuring error can be derived as

$$\frac{\tilde{\alpha}(x) - \alpha(x)}{\alpha(x)} = c\kappa \cdot \frac{x}{f_0}. \quad (21)$$

By use of Eqs. (20) and (16), the relative topography measuring error can be derived as

$$\frac{\tilde{z}(x) - z(x)}{z(x)} = \frac{2}{3} \cdot c\kappa \cdot \frac{x}{f_0}. \quad (22)$$

We now assume a more realistic measuring scenario where the SUT of length L is tilted in such a way that $z(0) = z(L) = 0$. This allows the autocollimator to use its full angle measuring range. The topography measuring error is then given by

$$\tilde{z}(x) - z(x) = \frac{c\kappa}{f_0 r} \cdot \left(\frac{x^3}{3} + \left(D_0 - \frac{L}{2} \right) \frac{x^2}{2} - \frac{D_0 L}{2} x \right). \quad (23)$$

Please note that Eqs. (20) and (23) describe the form measuring error due to changes in air pressure. When differences between measurements performed at different pressures are considered, the impact of pressure-independent optical aberrations of the autocollimator's objective is eliminated, see Sec. II D. In Secs. IV B and IV C, we demonstrated air pressure variations due to changes in weather and differing elevations of the labs of up to 89 hPa, which correspond to a relative pressure difference $\kappa = 0.089$ or approximately 9%. For a sensitivity c of the autocollimator's angle measurements of $c \approx 7.6 \cdot 10^{-4}$ ($c/p_0 \approx 0.75$ ppm/hPa), this results in a relative slope measuring error of the order of 67 ppm multiplied by $(x + D_0)/f_0$, with $f_0 = 300$ mm in case of the Elcomat 3000.

Figure 5 presents the topography measuring error of an autocollimator-based deflectometric profilometer according to Eq. (23) for the following parameters: SUT radius of curvature $r = 20$ m, SUT length $L = 0.25$ m, surface height variation of $3.9 \cdot 10^{-4}$ m peak-to-valley (pv), initial beam path length $D_0 = 0.5$ m, and relative pressure difference $\kappa = 0.089$ (89 hPa). Panel (a) of Fig. 5 presents the SUT slope, (b) the SUT topography, (c) the topography measuring error, and (d) the same topography measuring error after removal of its spherical component. As panel (c) of Fig. 5 demonstrates, the

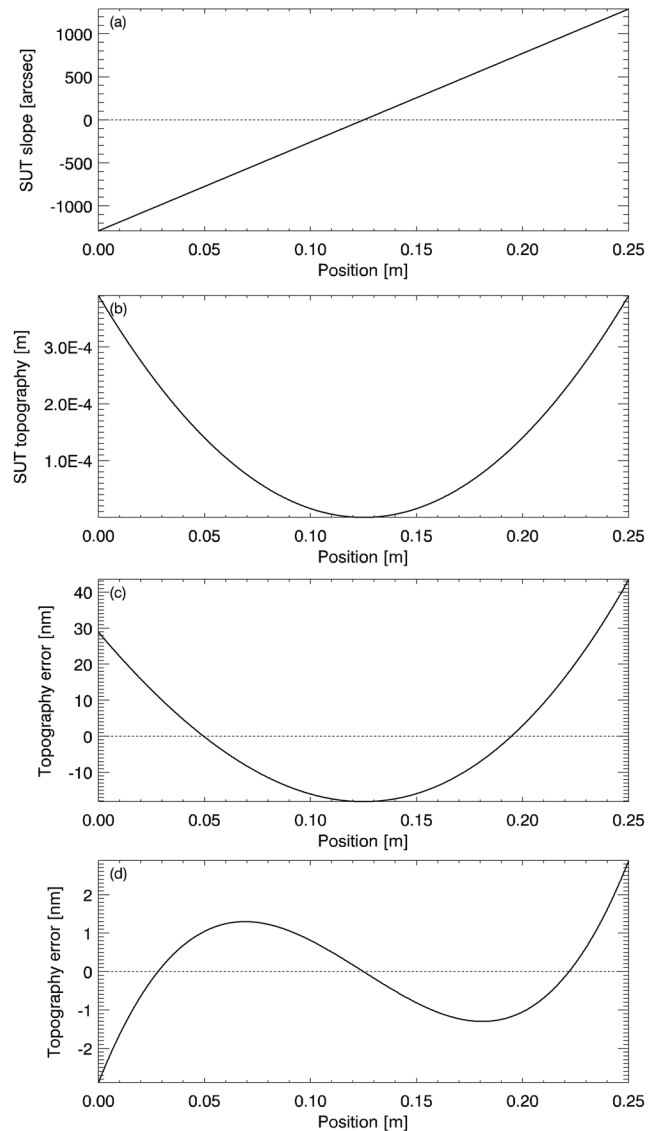


FIG. 5. Topography measuring error of a deflectometric profilometer caused by a difference in air pressure of 89 hPa. The SUT has a radius of curvature of $r = 20$ m and length $L = 0.25$ m. Panels: SUT slope (a) and topography (b), topography measuring error before (c) and after (d) removal of its spherical component.

main component of the topography measuring error is spherical (62 nm pv). The apparent radius of curvature of the SUT differs from its nominal value by $1.4 \cdot 10^{-4}$ (relative change). After removal of the spherical component, see panel (d), a third-order topography error of 5.8 nm pv remains.

Figure 6 presents the topography measuring error according to Eq. (23) for a larger SUT with a length of $L = 1$ m. The SUT radius is increased to $r = 80$ m so that its slope range is identical to the slope range of the SUT used for Fig. 5. The surface height variation increases to $1.6 \cdot 10^{-3}$ m pv. The remaining parameters, the initial beam path length

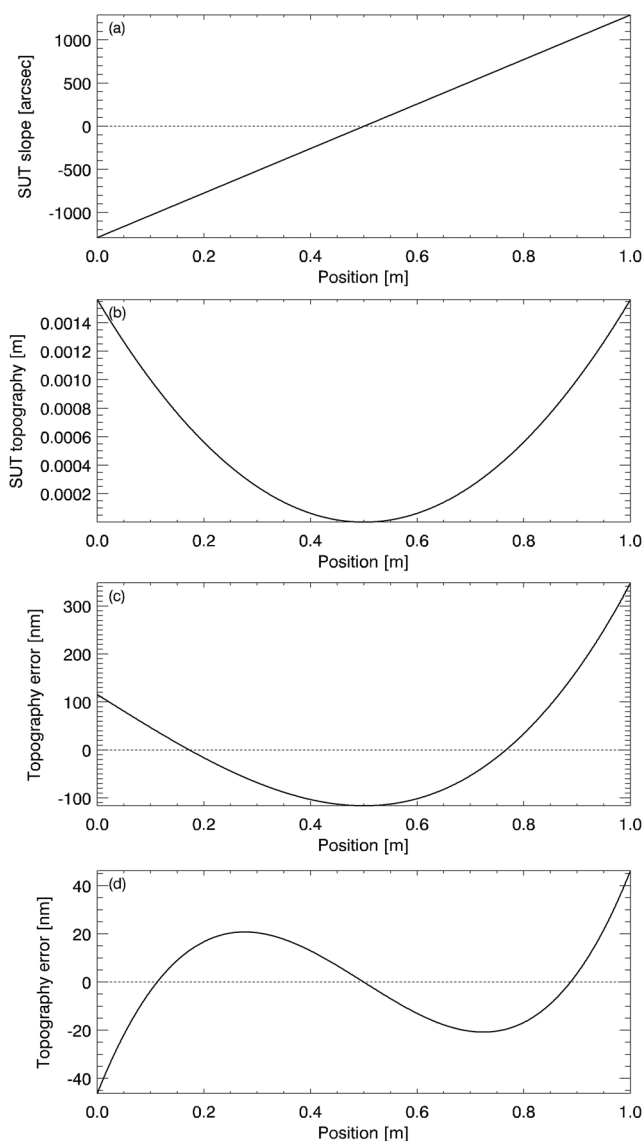


FIG. 6. Topography measuring error caused by a difference in air pressure of 89 hPa. The SUT has a radius of curvature of $r = 80$ m and length $L = 1$ m. Its slope range is identical to that of the SUT used for Fig. 5. Panels: SUT slope (a) and topography (b), topography measuring error before (c) and after (d) removal of its spherical component.

$D_0 = 0.5$ m and the relative pressure difference $\kappa = 0.089$ (89 hPa), remain unchanged. Panel (c) of Fig. 6 demonstrates the dominant spherical component of the topography measuring error (460 nm pv) again. The apparent radius of curvature of the SUT differs from its nominal value by $2.2 \cdot 10^{-4}$ (relative change). After removal of the spherical component, see panel (d), a third-order topography error of 92 nm pv remains.

A note on error removal. We assume that an identical trace on the SUT is measured in two different scanning directions: A–B and B–A, where A and B mark the beginning and the

end of the trace, respectively. As Eq. (23) demonstrates, the third-order component of the topography measuring error can then be eliminated from the redundant data set (by reversing the order of the second measurement and adding it to the first measurement). The second-order (spherical) error component, however, cannot be eliminated in this way. It is inseparable from the second-order component of the SUT topography.

Let us define the relative topography error as the peak-to-valley (pv) range of the topography measuring error divided by the pv range of the topography itself. For the stated parameters for SUT #1 (#2), we obtain a relative error in the topography measurement of the order of $1.6 \cdot 10^{-4}$ ($3.0 \cdot 10^{-4}$). When a best-fit sphere is subtracted from the error, a relative error of the order of $1.5 \cdot 10^{-5}$ ($5.9 \cdot 10^{-5}$) remains. As the numbers demonstrate, the absolute topography error cannot be neglected for strongly curved optical surfaces for the most demanding of applications, whereas for near-flat surfaces, the pressure influence is of negligible impact.

VI. GRADIENTS IN AIR PRESSURE AND TEMPERATURE

A. Impact of gradients on beam propagation

In this section, we derive the impact of gradients in the refractive index of air on the propagation of the autocollimator's measuring beam. For simplicity, we assume a beam that is propagating horizontally across a distance l and that the refractive index varies as a function of the height h above ground, i.e., perpendicular to the beam. As the wave front of the beam covers equal optical path lengths $n \cdot l$ in its medium of propagation per unit of time, its tilt angle ϕ is given by

$$\tan \phi = \frac{\partial l}{\partial h} = \frac{\partial l}{\partial n} \cdot \frac{\partial n}{\partial h}. \quad (24)$$

From the constancy of the optical path length $n \cdot l$ across the wave front, we obtain

$$\frac{\partial l}{\partial n} = -\frac{l}{n}. \quad (25)$$

From Eqs. (24) and (25), we can derive the radius of curvature R of the autocollimator beam by use of the relation $\tan \phi \approx l/R$ as

$$R = n \cdot \left| \frac{\partial n}{\partial h} \right|^{-1} \approx \left| \frac{\partial n}{\partial h} \right|^{-1}. \quad (26)$$

Because $(n - 1) \ll 1$, we may neglect the factor n without concern.

B. Pressure gradient

Air pressure decreases with increasing elevation above sea level. This pressure gradient causes the refraction of a propagating beam, which is well known in astronomy. The pressure gradient is vertical (i.e., it is oriented parallel to the gradient of the gravitational field) and corresponds to a gradient in the refractive index of the air. A wave front that advances perpendicular to the gradient in the horizontal direction will be tilted by an angle, which is proportional to the distance travelled. In case of a deflectometric profilometer,

the horizontal part of the autocollimator's measuring beam between the autocollimator and the pentaprism is affected, see Fig. 4. From Eq. (6), the derivative of the refractive index of air n with respect to its pressure p follows as

$$\frac{\partial n}{\partial p} = \frac{n-1}{p}. \quad (27)$$

As the pressure difference across a thin atmospheric slab balances its weight, the vertical pressure gradient is given by

$$\frac{\partial p}{\partial h} = -\rho \cdot g. \quad (28)$$

Here, ρ denotes the air density and g the gravitational acceleration. For the ISA,³⁶ $\rho = 1.2 \text{ kg} \cdot \text{m}^{-3}$ at ground level and $\partial p/\partial h = -0.12 \text{ hPa/m}$. According to Eq. (26), the vertical air pressure gradient results in the beam's radius of curvature R of

$$R = \left| \frac{\partial n}{\partial p} \cdot \frac{\partial p}{\partial h} \right|^{-1} = \frac{1}{n-1} \cdot \frac{p}{\rho g}. \quad (29)$$

For the ISA³⁶ at ground level, see Sec. IV C, and a refractive index of the air of $(n-1) \approx 3 \cdot 10^{-4}$ (calculated according to Ref. 33 for a wavelength of 640 nm), the wavefront of the beam is tilted by 6.5 milliarcsec (32 nrad) per meter horizontal path length l and the beam's radius of curvature is $R = 3.1 \cdot 10^7 \text{ m}$.

C. Temperature gradient

From Eq. (6), the derivative of the refractive index of air n with respect to its temperature T follows as

$$\frac{\partial n}{\partial T} = -\frac{n-1}{T}. \quad (30)$$

The temperature gradient then results in the beam's radius of curvature R of

$$R = \left| \frac{\partial n}{\partial T} \cdot \frac{\partial T}{\partial h} \right|^{-1} = \frac{T}{n-1} \cdot \left| \frac{\partial T}{\partial h} \right|^{-1}. \quad (31)$$

We use the ISA³⁶ at ground level, see Sec. IV C, and $(n-1) \approx 3 \cdot 10^{-4}$ (calculated for a wavelength of 640 nm). For a temperature gradient of 0.01 K/m, the wavefront of the beam is tilted by 21.5 milliarcsec (104 nrad) per meter horizontal path length l and the beam's radius of curvature is $R = 9.6 \cdot 10^6 \text{ m}$. For a temperature gradient of 0.1 K/m, we obtain $R = 9.6 \cdot 10^5 \text{ m}$.

D. Impact on deflectometric form measurement

In a deflectometric profilometer, the autocollimator beam covers the beam path twice, on its way to the SUT and on its return path after having been reflected by the SUT. Due to this double pass, the apparent SUT curvature due to gradients in air pressure and temperature is double the value for a single pass of the beam, while the radius of curvature is halved.

In Sec. VI B, we derived the beam deflection due to the vertical pressure gradient in the atmosphere. The wavefront of the beam is tilted by 6.5 milliarcsec (32 nrad) per meter horizontal path length and the beam's radius of curvature is $R = 3.1 \cdot 10^7 \text{ m}$. Therefore, in a deflectometric profilometer, the effective tilt angle of the returning beam is 13.0 milliarcsec

(64 nrad) per meter. When a perfectly flat SUT is measured, this leads to an apparent topography with an equivalent radius of $1.6 \cdot 10^7 \text{ m}$. We denote it as the deflectometric radius R_d , with $R_d = R/2$. For an SUT of 1 meter in length, this corresponds to a peak-to-valley topography error of 8 nm.

Considering current specifications for the most demanding synchrotron and XFEL beamline optics¹⁰⁻¹² and limits in their manufacturing and mounting, the effect size is currently too small to be of relevance. In the case of NMIs, however, which use deflectometric profilometry for the creation of large flatness standards for the traceable calibration of interferometers, the effect size is approaching the standard uncertainties stated by some NMIs, e.g., Refs. 8 and 9. In the case of flatness standards, the absolute form error is relevant, including its spherical component.

By use of Eqs. (24)–(26), from the beam's radius of curvature R , we can derive the pv slope measuring error of a deflectometric profilometer as

$$\text{pv}\{\tilde{\alpha}(x) - \alpha(x)\}|_{x=0}^L = \frac{L}{R_d} = 2 \cdot \frac{L}{R}. \quad (32)$$

Here, L is the SUT length and $\tilde{\alpha}(x) - \alpha(x)$ is the difference between the measured and the real SUT slope. Equation (32) already accounts for the above-mentioned fact that, in a deflectometric profilometer, the horizontal autocollimator beam effectively covers twice the SUT length. The root-mean-squared (rms) slope measuring error is given as

$$\text{rms}\{\tilde{\alpha}(x) - \alpha(x)\}|_{x=0}^L = \frac{1}{\sqrt{3}} \cdot \frac{L}{R_d} = \frac{2}{\sqrt{3}} \cdot \frac{L}{R}. \quad (33)$$

By use of the equation for the sagittal height of a circular segment from basic geometry, from the beam's radius of curvature R , we can derive the pv topography measuring error of a deflectometric profilometer as

$$\text{pv}\{\tilde{z}(x) - z(x)\}|_{x=0}^L = \frac{L^2}{8R_d} = \frac{L^2}{4R}. \quad (34)$$

Here, $\tilde{z}(x) - z(x)$ is the difference between the measured and the real SUT topography.

Table I reviews the impact of different gradients in air pressure and temperature on the propagation of the autocollimator beam and the deflectometric radius measured by a profilometer. Please note that, for a deflectometric profilometer that measures a SUT face up, see Fig. 4, the pressure gradient affects the slope measurement in the sagittal plane, i.e., the form measurement is affected directly. In case of a setup that measures the SUT in side-facing orientation, however, the pressure gradient affects the slope measurement in the transversal plane only. Also note that gradients in air pressure and temperature affect the form measurement of both strongly curved and flat SUT in the same manner and that the form measuring error increases quadratically with the length of the SUT.

As the numbers demonstrate, the refraction of the autocollimator's beam by the unavoidable atmospheric pressure gradient and by small gradients in air temperature at the

TABLE I. Impact of different gradients in air pressure and temperature on beam propagation.

Parameter	Gradient	Beam deflection	Beam radius R (m)	Deflectometric radius ^a R _d (m)
Pressure	$\partial p/\partial h = -0.12$ hPa/m	6.5 milliarcsec/m (32 nrad/m)	$3.1 \cdot 10^7$	$1.6 \cdot 10^7$
	$\partial T/\partial h = 0.001$ K/m	2.2 milliarcsec/m (10 nrad/m)	$9.6 \cdot 10^7$	$4.8 \cdot 10^7$
Temperature	$\partial T/\partial h = 0.01$ K/m	21.5 milliarcsec/m (0.1 μ rad/m)	$9.6 \cdot 10^6$	$4.8 \cdot 10^6$
	$\partial T/\partial h = 0.1$ K/m	0.2 arc sec/m (1.0 μ rad/m)	$9.6 \cdot 10^5$	$4.8 \cdot 10^5$

^aThe radius R_d detected by a deflectometric profilometer is half the beam radius R, see text.

level of a few milli-Kelvin per meter results in form measuring errors, which can approach or surpass tolerances specified for the most demanding optical surfaces, such as traceable flatness standards for interferometer calibration, large (meter-sized) astronomical optics, optics for extreme ultraviolet lithography, or synchrotron and XFEL beamline optics.

VII. IMPACT OF TEMPERATURE ON ANGLE METROLOGY WITH AUTOCOLLIMATORS

In this section, we analyze the impact of temperature changes on the angle metrology by use of autocollimators. To this purpose, we examine several thermal effects on the autocollimator, notably (a) temperature-induced changes in the refractive index of the air, (b) the thermal expansion of the frame on which its objective and the detector are mounted, (c) temperature-induced changes in the refractive index of the optical glass of its objective, (d) temperature-induced changes in its beam splitter, and (e) the thermal expansion of its detector.

A. Temperature-induced changes in the air's refractive index

The autocollimator type Elcomat High Resolution (HR), MWO, features a base manufactured from low expansion ceramics.³⁴ In this case, the thermal expansion of the autocollimator is minimal, while dominant changes in the refractive index of air are present. For analyzing the exclusive influence of changes in air temperature on the relative angle measuring error η , we make use of Eq. (9) and assume a constant pressure $p = p_0$ and humidity. We then obtain

$$\eta = c \cdot \frac{T_0 - T}{T} \cdot \frac{D}{f_0} \approx -c \cdot \frac{T - T_0}{T_0} \cdot \frac{D}{f_0}, \quad (35)$$

with the sensitivity c given by Eq. (11) again. Note that, in the divisor of Eq. (35), we can replace T with T_0 without concerns. By use of the ISA standard atmosphere at sea level, with $T_0 = 288.15$ K, we can evaluate the temperature sensitivity as $c/T_0 \approx c/T = 2.8$ ppm/K, with its associated standard uncertainty $u_{c/T_0} \approx 0.35$ ppm/K. However, note the minus sign on the right-hand side of Eq. (35). Therefore, $\partial\eta/\partial T = -c/T_0 = -2.8$ ppm/K, multiplied by the distance-dependent term in Eq. (35).

As far as the topography measuring error according to Eq. (23) is concerned, by redefining

$$\kappa = \frac{T_0 - T}{T} \approx -\frac{T - T_0}{T_0}, \quad (36)$$

as the relative temperature difference, instead of the relative pressure difference, we can reuse Eqs. (20)–(23) for evaluating its impact. As noted, Eq. (35) accounts for the impact of air temperature only. Additional thermal effects are described in Secs. VII B–VII F.

B. Thermal expansion of the autocollimator frame

In contrast to the autocollimator type Elcomat HR from MWO, which features a base manufactured from low expansion ceramics, the Elcomat 3000 features a steel mounting frame. We assume that the frame on which the autocollimator's objective and the detector are mounted places them at a distance $L_0 = f_0$ equal to the focal length f_0 of the objective at temperature T_0 . When the temperature changes from T_0 to T , the distance L is then given by

$$L = (1 + \gamma_{\text{frame}} \cdot (T - T_0)) \cdot f_0, \quad (37)$$

with γ_{frame} being the linear expansion coefficient of the frame, with a value of approx. 10 ppm/K–17 ppm/K for stainless steel.³⁸ When compared to temperature-induced changes in the air's refractive index, see Sec. VII A, the impact of the thermal expansion of the frame on the relative angle measuring error η is larger by a factor of 4 to 6. Therefore, we may neglect changes in the air's refractive index and make use of Eq. (3). When the temperature changes to T_0 , the resulting relative angle measuring error η is then given by

$$\eta = \gamma_{\text{frame}} \cdot (T - T_0) \cdot \left(1 - \frac{D}{f_0}\right). \quad (38)$$

For a SUT distance $D \neq f_0$, a relative angle measuring error $\eta \neq 0$ results. For stainless steel, $\partial\eta/\partial T$ is of the order of 10 ppm/K–17 ppm/K, multiplied by the distance-dependent term in Eq. (38).

C. Temperature-induced changes in the objective

The refractive index of optical glass depends on its temperature.³⁹ When it changes, the focal length of the objective

of autocollimator and its angle measurement are affected. We generalize Eq. (7) by introducing a temperature-dependent absolute (i.e., relative to the vacuum) refractive index n_g of the bulk material of the lens, with $n_g = n_g(T, p)$ and $n_{g0} = n_g(T_0, p_0)$. The change in focal length from f_0 to f is then given by

$$\frac{f}{f_0} = \frac{n}{n_0} \cdot \frac{n_{g0} - n_0}{n_g - n}. \quad (39)$$

In the case of changes in the refractive indices of air and glass, the relative angle measuring error η is then given by the modified Eq. (8) as

$$\eta = \frac{n \cdot n_{g0} - n_0 \cdot n_g}{n(n_{g0} - n_0)} \cdot \frac{D}{f_0}. \quad (40)$$

For changes in the refractive index of glass as a function of small temperature changes, we use a linear approximation

$$n_g - n_{g0} \approx \frac{n_{g0}^2 - 1}{2n_{g0}} \cdot d_0 \cdot (T - T_0) = \varepsilon_{glass} \cdot (T - T_0). \quad (41)$$

Here, d_0 is a constant which depends on the glass type (it is denoted D_0 in the literature; however, we want to avoid confusion with the distance that we have introduced in Sec. V). The comprehensive theory can be found, e.g., in Ref. 39. For a common optical glass, Schott N-BK7, the green Hg e-line at 546.1 nm (the line in the product catalog closest to the wavelength of the autocollimator illumination), and a temperature range of +20 °C to +40 °C, ε_{glass} is of the order of $1.6 \cdot 10^{-6}/K$, with $n_{g0} \approx 1.519$.⁴⁰ Note that this value characterizes the change in the absolute refractive index of this optical glass. The change in the relative optical index with respect to the refractive index of air, which also depends on temperature, is $3.0 \cdot 10^{-6}/K$.

As we have already considered temperature-induced changes in the refractive index of air, in Eq. (40), we set $n = n_0$. By use of Eq. (41), we obtain the relative angle measuring error η in the case of temperature-induced changes in the refractive index of the objective's glass as

$$\eta = -\frac{\varepsilon_{glass}}{n_{g0} - n_0} \cdot (T - T_0) \cdot \frac{D}{f_0}. \quad (42)$$

Note the minus sign in Eq. (42). With the specifications cited for Schott N-BK7, $\partial\eta/\partial T = -3.1$ ppm/K, multiplied by the distance-dependent term in Eq. (42).

When the temperature of the objective changes, its dimensions change along with its focal length. The interaction of this dimensional change with the constraints imposed by the mounting of the objective's lenses is beyond the scope of this article. Instead, we assume that the objective can change its dimensions free of constraints so that its focal length scales with its dimensions. By use of Eq. (4), we then obtain the relative angle measuring error η in the case of the thermal expansion of the objective's glass as

$$\eta = \gamma_{glass} \cdot (T - T_0) \cdot \frac{D}{f_0}, \quad (43)$$

with γ_{glass} being the linear expansion coefficient of the glass. Here, we made use of an approximation based on

$\gamma_{glass} \cdot (T - T_0) \ll 1$. For a common optical glass, Schott N-BK7, $\gamma_{glass} = 7.1$ ppm/K in the temperature range of -30 °C to +70 °C,⁴⁰ which results in $\partial\eta/\partial T = 7.1$ ppm/K, multiplied by the distance-dependent term in Eq. (43).

D. Temperature-induced changes in the beam splitter

In Sec. II E, we have discussed the beam splitter which displaces the focal plane of the autocollimator's objective according to Eq. (5) but does not affect the its focal length. For the sake of brevity, we do not derive an analytical expression for this minor environmental influence. Instead, we use Eq. (6) for calculating the change in the refractive index of the air, Eq. (37) for calculating the thermal expansion of the beam splitter, and Eq. (41) for calculating the change in its absolute refractive index. The impact of the changes is then analyzed numerically by inserting the values into Eq. (3). When deriving this equation, we have assumed that the detector is initially in the displaced focal plane, that the objective's focal length is constant, and that it is used for the conversion of the image shift to angle.

When the temperature changes from T_0 to T , we can then derive a linear approximation for the relative angle measuring error η due to temperature-induced changes in the beam splitter and the ambient air,

$$\eta \approx q_{bs} \cdot (T - T_0) \cdot \frac{d}{f_0} \cdot \left(1 - \frac{D}{f_0}\right). \quad (44)$$

Here, d is the total path length of the returning autocollimator beam in the beam splitter(s). The thermal expansion of the glass is characterized by its linear expansion coefficient γ_{glass} , with a value of 7.1 ppm/K for the optical glass Schott N-BK7 in the temperature range -30 °C to +70 °C. For the Hg e-line at 546.1 nm and a temperature range of +20 °C to +40 °C, its absolute refractive index changes by $1.6 \cdot 10^{-6}/K$, with $n_{g0} \approx 1.519$.⁴⁰ These parameters result in $q_{bs} = -3.7$ ppm/K. For a typical autocollimator, we may assume $d/f_0 \approx 0.1$, the approximate value for the Elcomat 3000. This results in $\partial\eta/\partial T = -0.4$ ppm/K, multiplied by the distance-dependent term in Eq. (44).

E. Thermal expansion of the CCD detector

The angle measurement by an autocollimator is based on assessing the shift of the reticle image on its CCD detector, which acts as a (relatively) stable metrological frame for measuring small, subpixel shifts. When the temperature increases, the CCD expands and the image shift appears to be reduced. The relative angle measuring error η of the autocollimator is then given by

$$\eta \approx -\gamma_{CCD} \cdot (T - T_0), \quad (45)$$

with γ_{CCD} being the linear expansion coefficient of the CCD. Here, we made use of an approximation based on $\gamma_{CCD} \cdot (T - T_0) \ll 1$. Note the minus sign in Eq. (45). The linear expansion coefficient of silicon is 2.6 ppm/K,³⁸ which results in $\partial\eta/\partial T = -2.6$ ppm/K.

TABLE II. Review of different influences on angle metrology with autocollimators and their effect sizes.

Parameter	Impact	Sensitivity	Parameter range (pv)	Relative angle measuring error η (pv)
Pressure (air) weather changes	Refractive index of air, Sec. IV B	$0.75 \text{ ppm/hPa} \times D/f_0$	84 hPa ^a	$63 \text{ ppm} \times D/f_0$
Pressure (air) elevation (~0 m–700 m)	Refractive index of air, Sec. IV C	$0.75 \text{ ppm/hPa} \times D/f_0$	89 hPa	$67 \text{ ppm} \times D/f_0$
Humidity (air)	Refractive index of air, Sec. III A	$-0.1 \text{ ppm/hPa} \times D/f_0$	5.7 hPa	$-0.6 \text{ ppm} \times D/f_0$
Temperature (air)	Refractive index of air, Sec. VII A	$-2.8 \text{ ppm/K} \times D/f_0$	0.06 K	$-0.2 \text{ ppm} \times D/f_0$
	Thermal expansion of frame (steel), Sec. VII B	$17 \text{ ppm/K} \times (1 - D/f_0)$	0.06 K	$1.0 \text{ ppm} \times (1 - D/f_0)$
	Thermal expansion of CCD, Sec. VII E	-2.6 ppm/K	0.06 K	-0.2 ppm
Temperature (autocollimator)	Refractive index of glass (objective), Sec. VII C	$-3.1 \text{ ppm/K} \times D/f_0$	0.06 K	$-0.2 \text{ ppm} \times D/f_0$
	Thermal expansion of glass (objective), Sec. VII C	$7.1 \text{ ppm/K} \times D/f_0$	0.06 K	$0.4 \text{ ppm} \times D/f_0$
	Refractive index and thermal expansion of glass (beamsplitter) ^b , Sec. VII D	$-0.4 \text{ ppm/K} \times (1 - D/f_0)$	0.06 K	$-0.02 \text{ ppm} \times (1 - D/f_0)$
Temperature	All temperature-induced changes combined	$14.0 \text{ ppm/K} - 15.4 \text{ ppm/K} \times D/f_0$	0.06 K	$0.8 \text{ ppm} - 0.9 \text{ ppm} \times D/f_0$

^aTotal weather-related pressure range observed over a decade (2006–2016).

^bThe temperature-induced change in the refractive index of air is included.

F. Review of environmental influences and effect sizes

Table II presents a review of the different environmental influences on the angle metrology with autocollimators. The parameter ranges refer to the environmental data recorded over the course of a full year (2015, see Sec. III A) in PTB's clean room center. In the case of air pressure, however, we have increased the peak-to-valley variation (69 hPa in 2015) slightly to accommodate weather-related pressure changes observed over a decade-long period (84 hPa, 2006–2016, see Sec. IV B). The pressure changes due to different elevations of the NMI, which participated in our international key comparison on autocollimator calibration (89 hPa, see Sec. IV C), are of this magnitude too and were added to Table II as a separate entry. In the last row in Table II, we have combined the impact of all temperature-induced changes in the autocollimator and the ambient air. They have been separated into a component, which scales with the SUT distance in relation to the focal length of the autocollimator, D/f_0 , and one which is independent of it. In addition to adding up the separate contributions, we have calculated the impact of simultaneous parameter changes and found no discrepancies.

As Table II demonstrates, in well controlled lab environments, air pressure constitutes the most important environmental impact on the precision angle and form metrology by use of autocollimators. Pressure decreases with increasing elevation and is subject to substantial variation due to weather. When compared to other environmental influences,

it dominates them by nearly two orders of magnitude. This statement is based on environmental data obtained at PTB's clean room center, which features an exceptional temperature stability. However, while other labs may also stabilize temperature accurately, large interlaboratory differences in the absolute temperature at which measurements are performed may be present. Stable temperature differences of 1 K are not uncommon. For a systematic temperature difference of 1 K, when all temperature effects are combined, this results in a distance-independent relative angle measuring error η of 14.0 ppm and a distance-dependent error of -15.4 ppm , multiplied with D/f_0 . Note that the temperature-induced error is quite small for $D \approx f_0$, while the pressure-induced error increases linearly with D/f_0 .

The numbers in Table II demonstrate that, for achieving the form tolerances specified for optical surfaces for the most demanding applications, environmental parameters need to be maintained within tight tolerances. While temperature can be stabilized accurately in lab environments, pressure is usually not under control. It varies with elevation and weather. Its influence needs to be corrected by the strategies, which we have developed in Sec. IV.

VIII. NOTES ON ERROR SUPPRESSION

In this section, we discuss several innovative approaches to the suppression of the systematic form measuring errors analyzed in this article. Figure 4 demonstrates the setup of

the most common type of autocollimator-based profilometer. The path lengths of both the outgoing and the returning autocollimator beam (after being reflected by the SUT) are subject to substantial changes. As a result, the returning beam follows different paths through the autocollimator's optical components, see Fig. 1. The returning beam intersects the autocollimator's objective at a distance $s = D \cdot \tan(2\alpha)$ with respect to its optical axis, with D being the path length from the objective to the SUT and α being the SUT's tilt angle. From the viewpoint of geometrical optics, we can characterize the systematic angle measuring errors of the autocollimator by the parameters s and α instead of D and α . Two approaches for error avoidance are feasible: (#1) By keeping D constant, the systematic angle measuring errors of the autocollimator can be characterized as a function of α and can be used for correction. (#2) By keeping α near zero, changes in s can be minimized even if D changes substantially.

Approach #1 is used by the Extended Shear Angle Difference (ESAD) technique developed by PTB.^{41–45} It is based on the analysis of slope differences between points on the SUT, which are offset by lateral shears of several millimeters to centimeters, which correspond to the changes in D . Scanning of the SUT is realized by moving it under the shearing unit. The use of slope differences eliminates the whole-body tilting of the SUT when it is moved. Both approaches are used by the Exact Autocollimation Deflectometric Scanning (EADS) technique of PTB.⁵ It modifies the setup in Fig. 4 by mounting the SUT on a tilting stage. At each measuring point, the SUT is tilted so that the autocollimator is used as a nulling instrument, i.e., $\alpha = 0$ (approach #2). A secondary autocollimator is used for measuring the tilt angle of the SUT, with D being held constant (approach #1).

A novel deflectometric scanning concept developed by Advanced Light Source (ALS), Lawrence Berkeley National Laboratory, USA, also makes use of both approaches (to our best knowledge, the concept was first considered in Ref. 46 and implemented and published in Refs. 47–49). It modifies the setup in Fig. 4 by moving the autocollimator itself across the SUT (instead of the beam-deflecting pentaprism), which keeps D constant (approach #1). A secondary autocollimator is used for measuring the small (arc sec) angular errors of the primary autocollimator when it is moved (approach #2). The Universal Test Mirror (UTM) of ALS combines both approaches in an innovative way.^{20,21} First, the slope of the SUT is measured by a standard profilometer as shown in Fig. 4. The SUT is then replaced by the UTM, a compact unit consisting of a mirror mounted on a tilting stage together with an autocollimator for measuring the tilt angle (D is kept constant; approach #1). The UTM is comoved with the pentaprism of the profilometer and its tilt angles are adjusted iteratively until the original measurement is reproduced, including all systematic errors. A secondary autocollimator is used for measuring the small (arc-sec) angular errors of the UTM when it is moved (approach #2).

ALS proposed arrangements of measuring sequences, which allows one to eliminate not only linear, but also higher-order drifts due to, e.g., changes in the environment.⁵⁰ The approach was generalized by use of a correlation

analysis, which guides the selection of appropriate sequences of measurements by flipping, tilting, and shifting the SUT, the Advanced Optimal Scanning Strategy (AOSS), see Refs. 50–52 and 48.

As an endnote, we would like to share our thoughts on miscellaneous supplemental error suppression strategies. As far as the influence of the air pressure is concerned, in addition to the correction strategies that we have developed in Sec. IV, we propose to use the image size of the reticle on the detector of the autocollimator for the *in situ* determination and correction of the effective focal length of the autocollimator's objective. This article focuses on the investigation of systematic errors in deflectometric form measurement. An investigation of random errors due to air convection and turbulence can be found in Refs. 53 and 49. The ideas on their suppression by shielding the autocollimator beam from environmental influences may also be applicable to the suppression of air temperature gradients. Finally, the use of form measurements obtained with tilted or shifted SUT may allow us to extract the systematic errors (or rather the coefficients of their low-order polynomial descriptions) and to correct them.

IX. CONCLUSIONS

We have investigated the influence of environmental parameters on the slope and form metrology of optical surfaces by autocollimator-based deflectometric profilometers, which are in use in metrology labs worldwide. We have addressed the impact of changes in the pressure, temperature, and humidity of the ambient air (by their influence on the air's refractive index), as well as various temperature-induced changes in the autocollimator. Additionally, we have investigated the implications of gradients in air pressure and temperature.

In the field of precision angle and form metrology by use of autocollimators, air pressure constitutes the most important environmental factor. Pressure decreases with increasing elevation and is subject to substantial variation due to weather. When compared to other environmental influences, it dominates them by nearly two orders of magnitude. In comparison, in well-controlled lab environments, temperature-induced effects are of minor importance. In the case of substantial interlaboratory differences in the absolute temperature at which measurements are performed; however, the impact of temperature may need to be considered.

We could demonstrate that, for typical pressure changes due to weather and elevation, relative slope and form measuring errors of the order of several 10^{-4} are to be expected. As the numbers demonstrate, in the case of strongly curved optical surfaces for the most demanding applications in optics, the absolute topography error can be of significance.

In this article, we have provided the community with the tools necessary for correcting the impact of pressure changes. When measurements are performed by use of deflectometric profilometers, we recommend monitoring the ambient air pressure along with other environmental parameters (such as the temperature and humidity of the air) and to state them

in the documentation accompanying each measurement. We have already proposed this procedure in a recent best practice guide.⁵⁴

ACKNOWLEDGMENTS

P.K. would like to thank František Dvořáček from CMI for his support and comments.

M.S. would like to thank Dirk Bastam for providing environmental data recorded at PTB's clean room center.

The IGMU of CMI and the SAAC of PTB were built within the EMRP Angle Metrology project (No. SIB58). The EMRP is jointly funded by the EMRP participating countries within EURAMET and the European Union.

The CMI participation in this project is cofunded by the Ministry of Education, Youth and Sports of the Czech Republic (Project No. 7AX13030).

The Advanced Light Source is supported by the Director, Office of Science, Office of Basic Energy Sciences, Material Science Division, of the U.S. Department of Energy under Contract No. DE-AC02-05CH11231 at Lawrence Berkeley National Laboratory.

This document was prepared as an account of work sponsored by the United States Government. While this document is believed to contain correct information, neither the United States Government nor any agency thereof, nor the Regents of the University of California, nor any of their employees make any warranty, express or implied, or assumes any legal responsibility for the accuracy, completeness, or usefulness of any information, apparatus, product, or process disclosed, or represents that its use would not infringe privately owned rights. Reference herein to any specific commercial product, process, or service by its trade name, trademark, manufacturer, or otherwise does not necessarily constitute or imply its endorsement, recommendation, or favoring by the United States Government or any agency thereof or the Regents of the University of California. The views and opinions of authors expressed herein do not necessarily state or reflect those of the United States Government or any agency thereof or the Regents of the University of California.

REFERENCES

- ¹Optical Shop Testing, 2nd ed., edited by D. Malacara (John Wiley & Sons, Inc., New York, 1992).
- ²See www.anglemetrology.com for EURAMET/EU project EMRP SIB 58 Angle Metrology.
- ³F. Siewert, H. Lammert, and T. Zeschke, in *Modern Developments in X-ray and Neutron Optics*, edited by A. I. Erko, M. Idir, T. Krist, and A. G. Michette (Springer, Berlin, 2008), Vol. 137, pp. 193–200.
- ⁴V. V. Yashchuk, S. Barber, E. E. Domning, J. L. Kirschman, G. Y. Morrison, B. V. Smith, F. Siewert, T. Zeschke, R. Geckeler, and A. Just, *Nucl. Instrum. Methods Phys. Res., Sect. A* **616**, 212 (2010).
- ⁵M. Schulz, G. Ehret, and A. Fitzenreiter, *J. Eur. Opt. Soc. Rapid Publ.* **5**, 10026 (2010).
- ⁶F. Siewert, J. Buchheim, T. Zeschke, G. Brenner, S. Kapitzki, and K. Tiedtke, *Nucl. Instrum. Methods Phys. Res., Sect. A* **635**, S52–S57 (2011).
- ⁷F. Siewert, J. Buchheim, S. Boutet, G. J. Williams, P. A. Montanez, J. Krzywinski, and R. Signorato, *Opt. Express* **20**, 4525 (2012).
- ⁸G. Ehret, M. Schulz, M. Stavridis, and C. Elster, *Meas. Sci. Technol.* **23**, 94007 (2012).
- ⁹Y. Bitou and Y. Kondo, *Appl. Opt.* **55**, 9282 (2016).
- ¹⁰L. Samoylova, H. Sinn, F. Siewert, H. Mimura, K. Yamauchi, and T. Tschentscher, “Requirements on hard x-ray grazing incidence optics for European XFEL. Analysis and simulation of wavefront transformations,” *Proc. SPIE* **7360**, 73600E (2009).
- ¹¹H. Sinn, J. Gaudin, L. Samoylova, A. Trapp, and G. Galasso, X-ray Optics and Beam Transport, <https://edmsdirect.desy.de/item/D00000002081421>, European X-Ray Free-Electron Laser Facility GmbH, Hamburg, 2011.
- ¹²D. Mills and H. Padmore, in *X-ray Optics for BES Light Source Facilities Report of the Basic Energy Sciences Workshop on X-ray Optics for BES Light Source Facilities* (U.S. Department of Energy, Office of Science, Potomac, MD, 2013).
- ¹³R. D. Geckeler, A. Just, M. Krause, and V. V. Yashchuk, *Nucl. Instrum. Methods Phys. Res., Sect. A* **616**, 140 (2010).
- ¹⁴T. Yandayan, R. D. Geckeler, and F. Siewert, *Proc. SPIE* **9206**, 92060F (2014).
- ¹⁵R. D. Geckeler, M. Krause, A. Just, O. Kranz, and H. Bosse, *Measurement* **73**, 231 (2015).
- ¹⁶R. D. Geckeler, *Meas. Sci. Technol.* **18**, 115 (2007).
- ¹⁷S. K. Barber, G. Y. Morrison, V. V. Yashchuk, M. V. Gubarev, R. D. Geckeler, J. Buchheim, F. Siewert, and T. Zeschke, *Proc. SPIE* **7801**, 780103 (2010).
- ¹⁸S. K. Barber, V. V. Yashchuk, R. D. Geckeler, M. V. Gubarev, J. Buchheim, F. Siewert, and T. Zeschke, *Opt. Eng.* **50**, 073602 (2011).
- ¹⁹S. K. Barber, G. Y. Morrison, V. V. Yashchuk, M. V. Gubarev, R. D. Geckeler, J. Buchheim, F. Siewert, and T. Zeschke, *Opt. Eng.* **50**, 053601 (2011).
- ²⁰V. V. Yashchuk, W. R. McKinney, T. Warwick, T. Noll, F. Siewert, T. Zeschke, and R. D. Geckeler, *Proc. SPIE* **6704**, 67040A (2007).
- ²¹R. D. Geckeler and A. Just, *Proc. SPIE* **7077**, 70770B (2008).
- ²²V. V. Yashchuk, N. A. Artemiev, G. Centers, A. Chaubard, R. D. Geckeler, I. Lacey, H. Marth, W. R. McKinney, T. Noll, F. Siewert, M. Winter, and T. Zeschke, *Rev. Sci. Instrum.* **87**, 051904 (2016).
- ²³R. D. Geckeler and A. Just, *Proc. SPIE* **6704**, 670407 (2007).
- ²⁴R. D. Geckeler, N. A. Artemiev, S. K. Barber, A. Just, I. Lacey, O. Kranz, B. V. Smith, and V. V. Yashchuk, *Rev. Sci. Instrum.* **87**, 051906 (2016).
- ²⁵S. Qian, R. D. Geckeler, A. Just, M. Idir, and X. Wu, *Nucl. Instrum. Methods Phys. Res., Sect. A* **785**, 206 (2015).
- ²⁶R. D. Geckeler, O. Kranz, A. Just, and M. Krause, *Adv. Opt. Technol.* **1**, 6 (2012).
- ²⁷O. Kranz, R. D. Geckeler, A. Just, M. Krause, and W. Osten, *Adv. Opt. Technol.* **4**, 397 (2015).
- ²⁸A. Just, M. Krause, R. Probst, and R. Wittekopf, *Metrologia* **40**, 288 (2003).
- ²⁹R. D. Geckeler, P. Křen, A. Just, M. Schumann, and M. Krause, *Meas. Sci. Technol.* **29**, 75002 (2018).
- ³⁰E. Hecht, *Optics*, 3rd ed. (Addison-Wesley, Boston, Massachusetts, 1998).
- ³¹J. E. Greivenkamp, *Field Guide to Geometrical Optics* (SPIE, Bellingham, WA, 2004).
- ³²B. Edlén, *Metrologia* **2**, 71 (1966).
- ³³K. P. Birch and M. J. Downs, *Metrologia* **30**, 155 (1993).
- ³⁴See www.haag-streit.com/moeller-wedel-optical/products/electronic-autocollimators/elcomat-series/ for information on the Elcomat series of autocollimators.
- ³⁵See www.bipm.org/en/publications/guides/gum.html for JCGM 100:2008 Evaluation of Measurement Data—Guide to the Expression of Uncertainty in Measurement, ISO, Geneva, 2008.
- ³⁶ISO 2533:1975 International Standard Atmosphere, ISO, Geneva, 1975.
- ³⁷R. D. Geckeler, A. Just, V. Vasilev, E. Prieto, F. Dvořáček, S. Zelenika, J. Przybylska, A. Duta, I. Victorov, M. Pisani, F. Saraiva, J.-A. Salgado, S. Gao, T. Anusorn, S. L. Tan, P. Cox, T. Watanabe, A. Lewis, K. P. Chaudhary,

- R. Thalmann, E. Banreti, A. Nurul, R. Fira, T. Yandayan, K. Chekirda, R. Bergmans, and A. Lassila, *Metrologia* **55**, 4001 (2018).
- ³⁸K. Lüders and G. von Oppen, *Lehrbuch der Experimentalphysik*, Band 1 Mechanik, Akustik, Wärme (De Gruyter, Berlin, 2008).
- ³⁹Technical Information TIE-19 2016 Temperature Coefficient of the refractive Index, Schott AG, Mainz, 2016.
- ⁴⁰Schott Optical Glass Data Sheets 2017, Schott AG, Mainz, 2017.
- ⁴¹I. Weingaertner, M. Schulz, and C. Elster, *Proc. SPIE* **3782**, 306–317 (1999).
- ⁴²R. D. Geckeler and I. Weingaertner, *Proc. SPIE* **4779**, 1–12 (2002).
- ⁴³R. D. Geckeler, A. Just, R. Probst, and I. Weingärtner, *Tech. Mess.* **69**, 535 (2002).
- ⁴⁴M. Wurm and R. D. Geckeler, *Proc. SPIE* **5457**, 401–410 (2004).
- ⁴⁵R. D. Geckeler, *Proc. SPIE* **6317**, 63171H (2006).
- ⁴⁶V. V. Yashchuk, *Oral Presentation at the First Meeting on Development of a New Optical Surface Slope Measuring System—OSMS-I* (ALS, Berkeley, 2010).
- ⁴⁷S. Qian and M. Idir, *Proc. SPIE* **9687**, 96870D (2016).
- ⁴⁸I. Lacey, J. Adam, G. P. Centers, G. S. Gevorkyan, S. M. Nikitin, V. V. Yashchuk, and B. Smith, *Proc. SPIE* **10385**, 103850G (2017).
- ⁴⁹I. Lacey, K. Anderson, G. P. Centers, R. D. Geckeler, G. S. Gevorkyan, A. Just, T. Nicolot, B. V. Smith, and V. V. Yashchuk, *Proc. SPIE* **10760**, 1076002 (2018).
- ⁵⁰V. V. Yashchuk, *Rev. Sci. Instrum.* **80**, 115101 (2009).
- ⁵¹V. V. Yashchuk, G. Centers, G. S. Gevorkyan, I. Lacey, and B. V. Smith, *Proc. SPIE* **10612**, 106120O (2018).
- ⁵²V. V. Yashchuk, N. A. Artemiev, I. Lacey, and D. J. Merthe, *Proc. SPIE* **8848**, 88480I (2013).
- ⁵³V. V. Yashchuk, S. C. Irick, A. A. MacDowell, W. R. McKinney, and P. Z. Takacs, *Proc. SPIE* **6317**, 63170D (2006).
- ⁵⁴T. Yandayan, R. D. Geckeler, A. Just, F. Siewert, B. Grubert, E. Prieto, M. M. Pérez, M. Pisani, J. Przybylska, and R. Thalmann, Guidelines on the Calibration of Autocollimators EURAMET Calibration Guide No. 22, www.euramet.org, Euramet, Braunschweig, 2017.